

An Attempt to Produce Electrical Discharges in Acoustic Cavitation Bubbles^{*)}

Noriharu TAKADA, Yui HAYASHI¹⁾, Motonobu GOTO¹⁾ and Koichi SASAKI²⁾

Technical Center, Nagoya University, Nagoya 464-8603, Japan

¹⁾*Department of Chemical Engineering, Nagoya University, Nagoya 464-8603, Japan*

²⁾*Division of Quantum Science and Engineering, Hokkaido University, Sapporo 060-8628, Japan*

(Received 10 June 2016 / Accepted 23 August 2016)

It is widely known that cavitation bubbles are not static bubbles but have the dynamics of the expansion, the shrinkage, and the collapse. In this work, we produced electrical discharges in acoustic cavitation bubbles for the first time with the intension of enhancing the reactivity of sonochemical processes. Glow-like discharges were observed in cavitation bubbles on the bottom surface of the cylindrical electrode which was connected to a pulsed high-voltage power supply. Bright optical emission was observed from the region corresponding to the cloud of expanded cavitation bubbles, while we also observed electrical discharges even in the shrinking phase of cavitation bubbles. If discharge-produced reactive species have lifetimes that are longer than the interval between the discharge and the collapse of the cavitation bubble, the species composition in the collapsed cavitation bubble becomes different from that in conventional cavitation bubble, which may result in the enhancement of reactivity in sonochemical processes.

© 2016 The Japan Society of Plasma Science and Nuclear Fusion Research

Keywords: acoustic cavitation, glow-like discharge, temporal evolution, nonequilibrium sonochemistry

DOI: 10.1585/pfr.11.1406113

1. Introduction

Recently, electrical discharges inside bubbles in liquids attract much attention of many researchers in conjunction with pollution control [1, 2], sterilization [3, 4], treatments of biological tissues or plasma medicine [5, 6], and material processing [7]. In many cases, the power supply for the electrical discharges firstly produces bubbles via the Joule heating of the liquid, and it is followed by electrical discharges inside the bubbles [8–14]. Another way is the artificial introduction of bubbles from gas nozzles. A recent work by Tachibana has provided us clear pictures of the electrical discharge in an isolated bubble, which was produced by gas puffing from a nozzle [15]. This work has motivated the progress of numerical simulation on the formation of the electrical discharge inside a bubble in liquid [16].

In this work, we tried to produce electrical discharges inside cavitation bubbles for the first time. The cavitation bubble is a kind of bubble in liquid, but it has different features from the normal bubble produced by the gas puffing. A different point is the bubble dynamics. The bubble produced by the gas puffing is static, whereas the cavitation bubble has the dynamics of the expansion, the shrinkage, and the collapse [17]. The pressure inside the expanded cavitation bubble is lower than the liquid pressure, which is another different point from the normal bubble. The

shrinkage of the bubble is caused by the pressure difference between the bubble and the liquid.

The most important particularity of the cavitation bubble is the collapse. The inside of the cavitation bubble at the collapse has a high pressure and a high temperature because of the roughly adiabatic shrinkage. It is believed that a plasma is produced inside the cavitation bubble at the collapse [18, 19] (sometimes it is called “sonoplasma”) because of the high temperature. The particular physical parameters at the collapse of the cavitation bubble produces reactive radicals. The radicals are transported into the liquid, and they promote chemical reactions. This process is called “sonochemistry”.

It is considered that the plasma produced at the collapse of the cavitation bubble is close to a thermal plasma because of frequent collisions among particles. This is evident from the continuum spectra of the optical emission from the collapsed cavitation bubble or the sonoplasma [20–22]. On the other hand, electrical discharges can produce nonequilibrium plasmas, however, the electrical discharge in a cavitation bubble has never been tried yet. This work has an intention to change the reaction field at the collapse of the cavitation bubble from the thermodynamic equilibrium state to a nonequilibrium one. The electrical discharge in the expanded cavitation bubble produces reactive radicals. The chemical contents inside the collapsed cavitation bubble could be different if the shrinking cavitation bubble contains radicals produced by the discharge. In the paper, we report the characteristics of elec-

author's e-mail: sasaki@qe.eng.hokudai.ac.jp

^{*)} This article is based on the invited talk at the 32nd JSPF Annual Meeting (2015, Nagoya).

trical discharges inside acoustic cavitation bubbles.

2. Experimental Method

The experimental apparatus is schematically shown in Fig. 1. A rectangular vessel of $90 \times 90 \times 120 \text{ mm}^3$ was filled with distilled water with no gas bubbling. The vessel had three quartz windows on the sides for observing the cavitation bubbles and the optical emission from the discharge. An ultrasonic transducer was attached at the bottom of the vessel, and an electrical power (a sinusoidal wave) of 50 W at a frequency around 27 kHz was applied to the transducer to excite ultrasonic wave. The ultrasonic wave propagated from the bottom of the vessel toward the top surface of water. An aluminum punching plate with a surface area of $30 \times 30 \text{ mm}^2$ and a thickness of 1 mm was inserted from the top of water. The punching plate had many holes with 3 mm diameter. When the water depth, the position of the punching plate, and the frequency of the ultrasonic wave were optimized, we observed the efficient generation of cavitation bubbles at a distance of approximately 1 mm from the punching plate, as reported in a previous paper [23]. The diameter of the expanded cavitation bubble in the previous experiment, where we used an ultrasonic wave at 34 kHz, was approximately $100 \mu\text{m}$, but we could not identify the bubble size in the present experimental condition. The region with the concentrated formation of cavitation bubbles was standing, and the region with concentrated cavitation bubbles was seen like cloud by naked eyes because of the scattering of room lighting.

A cylindrical copper electrode of 1 mm diameter, which was covered with an alumina tube (1.2 mm inner diameter), was inserted into the cloud of concentrated cavitation bubbles. We observed that a part of cavitation bub-

bles was attached on the bottom surface of the electrode. A high-voltage power supply was connected to the electrode, while the punching plate was electrically grounded. The power supply yielded bipolar pulsed high voltage with a duration of approximately $3 \mu\text{s}$. The repetition frequency of the pulsed voltage was 10 kHz in the continuous oscillation mode, while the single pulse was supplied at a controlled timing with respect to the ultrasonic wave in the single-pulse experiment. A delay pulser was used for controlling the overlapping condition between the ultrasonic wave and the pulsed high voltage. Because of the high frequency and the small amplitude, the measurement of the discharge current using a current probe was difficult in this experiment.

The dynamics of cavitation bubbles were observed by shadowgraph imaging. The region with concentrated cavitation bubbles was illuminated by a Xe flash lamp from the radial direction of the cylindrical electrode, and the pattern of the transmitted lamp light was captured using a charge-coupled device camera with a gated image intensifier (ICCD camera). The same ICCD camera was used for observing the side image of the optical emission from the discharge. In addition, we also took the image of the optical emission from the discharge from the axial direction of the cylindrical electrode by moving the camera position. The timing of the gate opening of the ICCD camera was varied with respect to the waveforms of the ultrasonic wave and the high-voltage pulse using a delay pulser.

3. Results

Figure 2 shows the waveforms of the sinusoidal voltage applied to the ultrasonic transducer and the pulsed high voltage applied to the cylindrical electrode. The horizontal position of the discharge voltage in the figure was movable with respect to the ultrasonic sinusoidal voltage in the

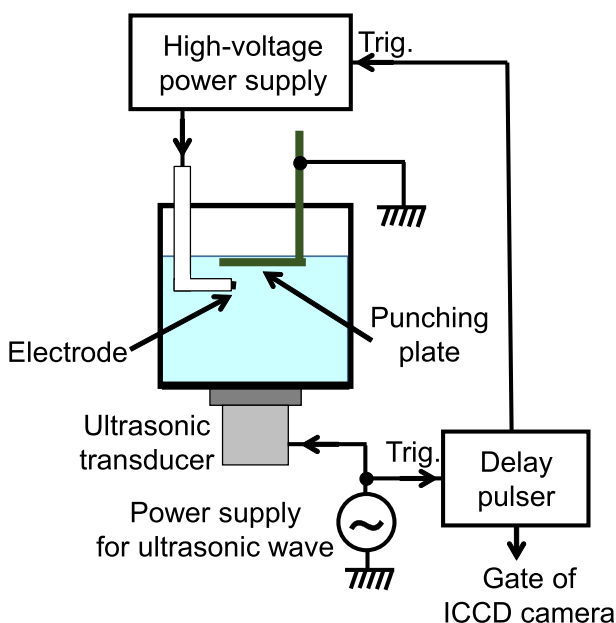


Fig. 1 Schematic of experimental apparatus.

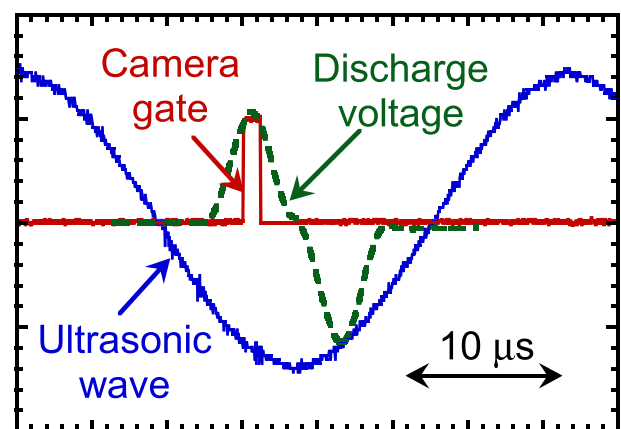


Fig. 2 Waveforms of the discharge voltage and the voltage applied to the ultrasonic transducer. The gate duration of the ICCD camera is also illustrated by the rectangular waveform.

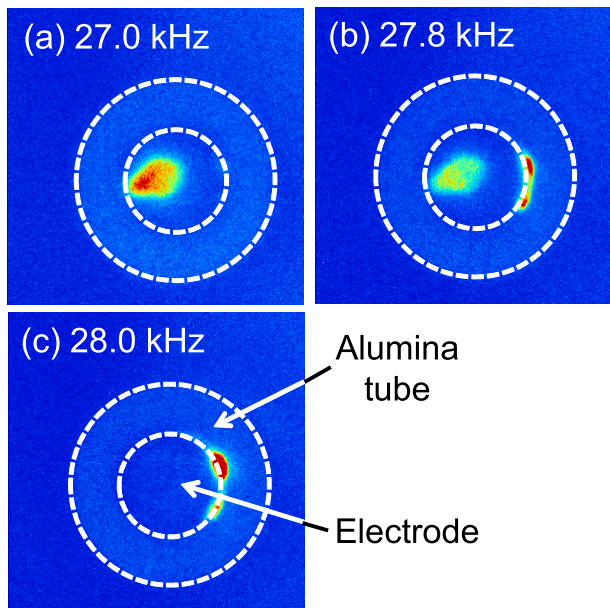


Fig. 3 Optical emission patterns observed on the bottom surface of the cylindrical electrode at ultrasonic frequencies of (a) 27.0, (b) 27.8, and (c) 28.0 kHz.

single-pulse experiment. The waveform of the gate opening shown in Fig. 2 has a duration of $1\ \mu\text{s}$, and was also movable with respect to the ultrasonic sinusoidal voltage and the pulsed high voltage.

The pictures of the optical emission image on the bottom surface of the cylindrical electrode are shown in Fig. 3. These pictures were taken from the axial direction of the cylindrical electrode when the frequency of the ultrasonic wave was varied between 27.0 and 28.0 kHz. The positions of the cylindrical electrode and the alumina tube are illustrated in the figures. The high-voltage power supply worked in the continuous mode. The duration of the gate opening was 1 s in these pictures, which was much longer than the cycle periods of both the ultrasonic wave and the high voltage. In other words, the overlapping condition between the waveforms of the high-voltage pulse and the ultrasonic wave changed randomly, and these pictures were obtained by accumulating the optical emission image on the ICCD camera for many cycles. The peak voltage of the pulsed power supply was 8 kV.

Since our method for producing concentrated cavitation bubbles was a resonant phenomena [23], the production efficiency was sensitive to the ultrasonic frequency when the water depth was fixed. In the experiment shown in Fig. 3, cavitation bubbles were produced efficiently at a frequency of 27.0 kHz. Cavitation bubbles are also produced weakly at a frequency of 27.8 kHz, while we did not observe cavitation bubbles at 28.0 kHz. When cavitation bubbles are produced, as shown in Fig. 3 (a), we observed the formation of glow-like discharge on a part of the bottom surface of the cylindrical electrode. The discharge color was pink. On the other hand, at a frequency

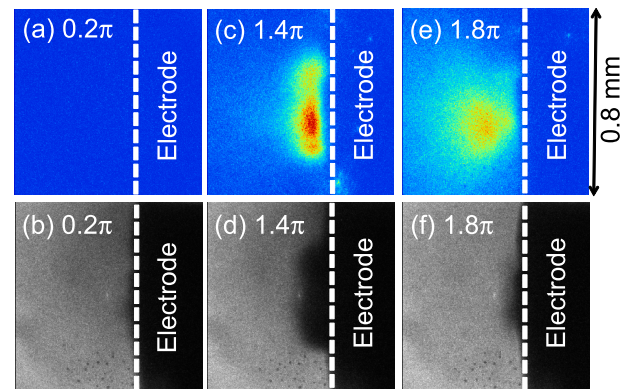


Fig. 4 Optical emission patterns ((a), (c), (e)) and shadowgraph images ((b), (d), (f)) observed from the side of the cylindrical electrode. The gate opening of the ICCD camera was synchronized with the positive peak of the discharge voltage. The trigger for gate opening was adjusted at relative phases of (a) and (b) 0.2π , (c) and (d) 1.4π , and (e) and (f) 1.8π .

of 28.0 kHz, where we did not observe cavitation bubbles, arc-like discharges were produced intermittently at the corner edge of the cylindrical electrode, as shown in Fig. 3 (c). The discharge color was white. We observed both the glow-like discharge on the bottom surface and the intermittent arc-like discharge at the corner edge of the electrode, when the frequency of the ultrasonic wave was 27.8 kHz, as shown in Fig. 3 (b).

Figure 4 shows side pictures of the optical emission from the discharge, together with the shadowgraph images of the cavitation bubble, when the frequency of the ultrasonic wave was 27.0 kHz. The position of the surface of the cylindrical electrode is illustrated by the dashed lines in the figures. When we took the shadowgraph images, the gate width of the ICCD camera was fixed at $1\ \mu\text{s}$, and the trigger pulse for the gate opening was varied at a step of $3.7\ \mu\text{s}$. In this way, we examined the temporal variation of the shadow area at 10 relative phases of the sinusoidal wave applied to the ultrasonic transducer. The high-voltage power supply was switched off in the experiment of shadowgraph imaging. When we took the pictures of the optical emission, the flash lamp for shadowgraph imaging was switched off, and the single high-voltage pulse was applied to the cylindrical electrode. The gate of the ICCD camera ($1\ \mu\text{s}$) was opened at the timing of the maximum voltage of the positive high-voltage pulse, as shown in Fig. 2, and the overlapping condition between the ultrasonic wave and the high-voltage pulse was varied at the same step of $3.7\ \mu\text{s}$ as that in the shadowgraph imaging. The pictures shown in Fig. 4 were obtained by accumulating the images on the ICCD camera 3×10^4 times.

At a relative phase of 0.2π , as shown in Fig. 4 (b), we observed a negligible shadow area, indicating that the cavitation bubbles were collapsed. The cavitation bubbles were

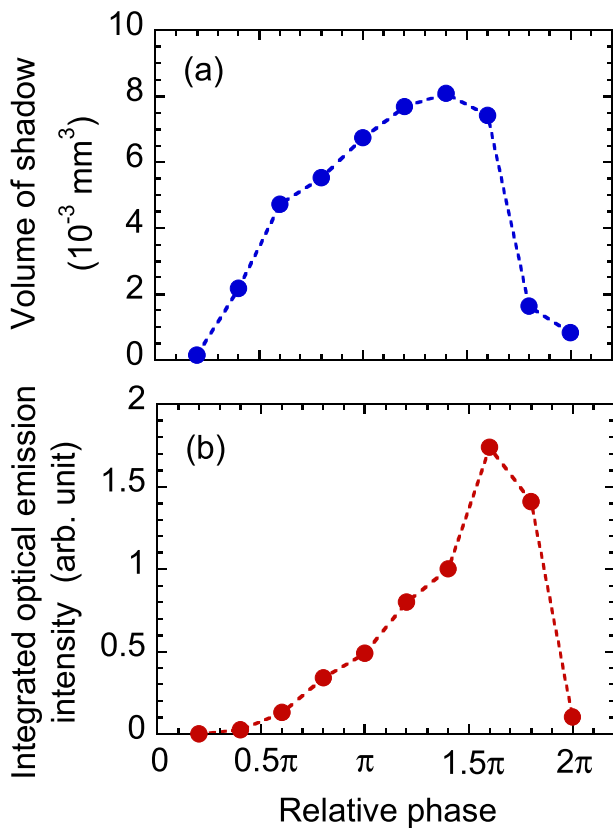


Fig. 5 (a) Volume of shadow and (b) integrated optical emission intensity as a function of the relative phase between the positive peak of the discharge voltage and the voltage applied to the ultrasonic transducer.

observed at later phases. The maximum shadow area was observed at a relative phase of 1.4π , as shown in Fig. 4 (d). It is noted here that the shadow shown in Fig. 4 (d) does not show a single cavitation bubble. The area corresponding to the shadow was seen like a white cloud by naked eyes due to scattering of room lighting, indicating that the shadow part is composed a number of small cavitation bubbles. The shadow area started to shrink after 1.4π . The shrunken shadow shown in Fig. 4 (f) was observed before the collapse. Since cavitation bubbles gather due to the secondary Bjerknes force, the shrinkage of the shadow area means the shrinkage of cavitation bubbles. We observed negligible optical emission at a phase corresponding to the collapsed cavitation bubble, as shown in Fig. 4 (a). The discharges were observed from the region corresponding to the shadow area in later relative phases between 0.4π and 1.4π . The optical emission image at the maximum shadow area is shown in Fig. 4 (c). In the shrinking phase of the cavitation bubbles, as shown in Fig. 4 (e), we observed optical emission from the outside of the shadow area.

Figure 5 shows the volume of the shadow area, which was evaluated from the shadowgraph images under the assumption of cylindrical symmetry, and the optical emission intensity, which was evaluated by integrated the op-

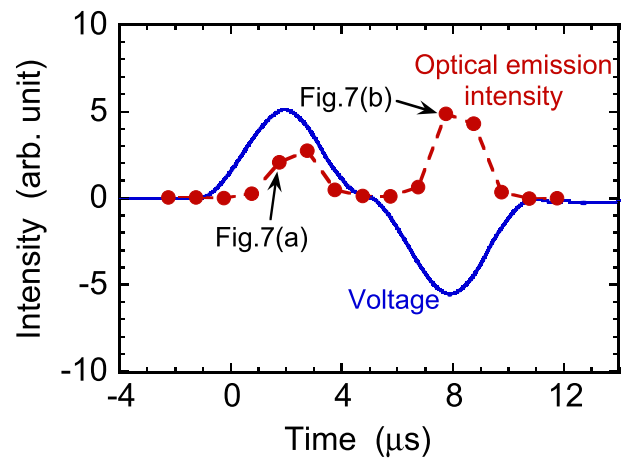


Fig. 6 Temporal variation of the integrated optical emission intensity, together with the waveform of the discharge voltage. The relative phase between the gate opening of the ICCD camera and the voltage applied to the ultrasonic transducer was fixed at 1.4π .

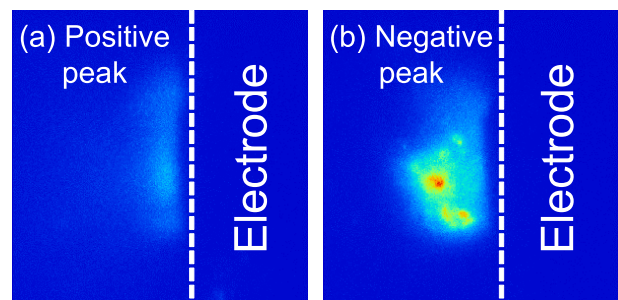


Fig. 7 Optical emission patterns observed from the side of the cylindrical electrode at the positive and negative peaks of the discharge voltage. The relative phase between the gate opening of the ICCD camera and the voltage applied to the ultrasonic transducer was fixed at 1.4π .

tical emission image, as a function of the relative phase between the ultrasonic wave and the positive-side peak of the high-voltage pulse. As shown in Fig. 5, the optical emission intensity increased with the volume of the bubble area between 0.2π and 1.4π . Interesting phenomena were observed at 1.6π and 1.8π , where higher optical emission intensities were observed even though the volume of the shadow area became smaller. The higher integrated optical emission intensity is mainly due to the optical emission from a wider area than the shadow area.

We fixed the overlapping condition between the ultrasonic wave and the gate opening of the ICCD camera at the relative phase of 1.4π , and we changed the overlapping condition between the gate opening of the ICCD camera and the waveform of the high-voltage pulse. As shown in Fig. 6, the integrated optical emission intensity had two peaks within a cycle of the high-voltage pulse, and the two peaks were observed at the maxima of the positive and neg-

ative high voltages. The optical emission intensity at the negative high voltage was higher than that at the positive high voltage. In addition, we observed the difference in the optical emission images in the positive and negative high voltages. Figures 7 (a) and 7 (b) shows the optical emission images at the maxima of the positive and negative pulse voltages (the data points indicated in Fig. 6). As shown in Fig. 7, the axial distribution of the optical emission intensity at negative pulsed voltage was wider than that at the positive voltage.

4. Discussion

The discharge produced on the bottom surface of the cylindrical electrode had a different aspect from the discharge at the corner edge, as shown in Fig. 3. The arc-like discharge was observed intermittently at the corner edge of the cylindrical electrode when the cavitation bubbles were not induced (Fig. 3 (c)). The arc-like discharge may be produced in a bubble which was induced by Joule heating of water in the area with the intense electric field. Since the electric field at the corner edge of the electrode is much higher than the discharge threshold in the bubble, the discharge occurs at “the spark mode” when the bubble is formed by the Joule heating, resulting in the arc-like bright discharge.

On the other hand, on the basis of the experimental results, we judged that the glow-like discharges were produced in the cavitation bubbles. This judgment is based on the spatial agreement between the areas of the optical emission and the cavitation bubbles, as shown in Figs. 3 and 4. We never observed the glow-like discharges on the bottom surface of the cylindrical electrode in the absence of the cavitation bubbles, even when we applied the ultrasonic power. It is well known that the threshold voltage to produce electrical discharge in gases is lower than that in liquids. In addition, the pressure inside an expanded cavitation bubble is generally understood to be on the order of 10^3 Pa [24]; hence the discharge can occur in the expanded cavitation bubbles even though the electric field is lower than that at the corner edge. Because of the lower electric field and the reduced gas pressure, the discharge occurs at “the streamer mode” or “the glow mode”. Since the discharge in the liquid phase among the cavitation bubbles is unlikely because of the high threshold voltage, we judged that the glow-like discharges were produced in the cavitation bubbles on the basis of the spatial agreement between the areas of the optical emission and the cavitation bubbles.

The spatial agreement between the areas of the optical emission and the cavitation bubble (the shadow area in the shadowgraph imaging) was observed in the relative phases between 0.4π and 1.4π . The integrated optical emission intensity correlated with the volume of the shadow area, as shown in Fig. 5, at the phases between 0.2π and 1.4π . The exceptions were observed at the phases of 1.6π and 1.8π . In these phases, as shown in Fig. 4 (e), we observed

the optical emission from the region corresponding to the outside of the shadow area. This may be explained by the possibility of dispersed small cavitation bubbles. The shadowgraph imaging used in the present experiment can capture the accumulated cavitation bubbles as the shadow in the transmitted light pattern, whereas it cannot detect an isolated cavitation bubble because of the insufficient spatial resolution. Figure 4 (e) suggests the existence of dispersed cavitation bubbles in the area with the optical emission from the discharge. Another mechanism could be discharges in bubbles induced by Joule heating. However, this is improbable since the ultrasonic water pressure (sinusoidal waveform) is higher than the atmospheric pressure in the shrinking phase of cavitation bubbles [24]. The formation of bubbles by Joule heating becomes less efficient at a higher water pressure because of a higher boiling temperature. Actually, it has been observed experimentally that the optical emission intensity from plasmas in bubbles induced by microwave heating becomes weaker at the higher ultrasonic pressure [14].

As shown in Fig. 6, the temporal variation of the optical emission intensity was similar to the temporal variation of the absolute value of the discharge voltage, indicating that the lifetime of the plasma inside the cavitation bubbles is shorter than $\sim 1 \mu\text{s}$. The short lifetime of the plasma may be owing to the small volume of the discharge area. The optical emission intensity in the negative-voltage phase was higher than that in the positive-voltage phase. In addition, as shown in Fig. 7, the discharge area in the negative-voltage phase was wider than that in the positive-voltage phase. The mechanism of the intenser discharge in the negative-voltage phase has not been understood yet, but it may be related to the difference between the positive and negative corona discharges. It is known that the electric field near the electrode is stronger in the negative corona discharge [25]. Since the discharge area in the present experiment is localized within ~ 0.3 mm from the electrode, a stronger electric field could be expected in the negative-voltage phase.

The principal intension of the present work was to introduce nonequilibrium effects into sonochemistry. As shown in Figs. 4 and 5, we succeeded in producing the discharge until $3.7 \mu\text{s}$ (0.2π) before the collapse of the cavitation bubble. The inside of the cavitation bubbles is occupied by water vapor in the case without the discharge. The discharge inside the cavitation bubbles may dissociate water vapor by electron impact dissociation $\text{H}_2\text{O} + e \rightarrow \text{OH} + \text{H} + e$. In addition, association reactions of OH radicals, $\text{OH} + \text{OH} + \text{M} \rightarrow \text{H}_2\text{O}_2 + \text{M}$ and $\text{OH} + \text{OH} \rightarrow \text{H}_2\text{O} + \text{H}$ produce additional reactive species. If the lifetimes of these reactive species are longer than $3.7 \mu\text{s}$, the species composition in the collapsed cavitation bubbles with the discharge is different from that without the discharge. Accordingly, we can expect a different reaction field in the collapsed cavitation bubble, and it may result in more reactive sonochemistry processes. In the next work, we will

examine the effect of the discharge on the characteristics of sonochemical material syntheses.

5. Conclusions

In this work, we produced electrical discharges in acoustic cavitation bubbles for the first time. Glow-like discharges were observed in cavitation bubbles which were attached on the bottom surface of the cylindrical electrode. The discharge was possible until $3.7\ \mu\text{s}$ before the collapse of the cavitation bubbles. If lifetimes longer than $3.7\ \mu\text{s}$ are expected for discharge-produced reactive species, the species composition inside the collapsed cavitation bubbles with the discharge may be different from that without the discharge. The discharge in the cavitation bubbles may be helpful to enhance the reactivity of sonochemistry processes.

Acknowledgments

The authors are grateful to Naoki Shirai for helpful discussion.

- [1] B.R. Locke, M. Sato, P. Sunka, M.R. Hoffmann and J.S. Chang, *Ind. Eng. Chem. Res.* **45**, 882 (2006).
- [2] B. Sun, M. Sato, A. Harano and J.S. Clements, *J. Electrostatics* **43**, 115 (1998).
- [3] M. Laroussi, *IEEE Trans. Plasma Sci.* **24**, 1188 (1996).
- [4] S. Ikawa, K. Kitano and S. Hamaguchi, *Plasma Process. Polym.* **7**, 33 (2010).
- [5] G. Fridman, G. Friedman, A. Gutsol, A.B. Shekhter, V.N. Vasilets and A. Fridman, *Plasma Process. Polym.* **5**, 503 (2008).
- [6] M.G. Kong, G. Kroesen, G. Morfill, T. Nosenko, T. Shimizu, J. van Dijk and J.L. Zimmermann, *New J. Phys.* **11**, 115012 (2009).
- [7] T. Ishijima, K. Nosaka, Y. Tanaka, Y. Uesugi, Y. Goto and H. Horibe, *Appl. Phys. Lett.* **103**, 142101 (2013).
- [8] P. Bruggeman and C. Leys, *J. Phys. D: Appl. Phys.* **42**, 053001 (2009).
- [9] K. Sato and K. Yasuoka, *IEEE Trans. Plasma Sci.* **36**, 1144 (2008).
- [10] P. Bruggeman, J. Degroote, J. Vierendeels and C. Leys, *Plasma Sources Sci. Technol.* **17**, 025008 (2008).
- [11] T. Ishijima, H. Hotta and H. Sugai, *Appl. Phys. Lett.* **91**, 121501 (2007).
- [12] T. Ishijima, H. Sugiura, R. Saito, H. Toyoda and H. Sugai, *Plasma Sources Sci. Technol.* **19**, 015010 (2010).
- [13] T. Shirafuji and Y. Himeno, *Jpn. J. Appl. Phys.* **52**, 11NE03 (2013).
- [14] T. Takahashi, T. Takada and H. Toyoda, *Jpn. J. Appl. Phys.* **53**, 07KE01 (2014).
- [15] K. Tachibana, Y. Takekata, Y. Mizumoto, H. Motomura and M. Jinno, *Plasma Sources Sci. Technol.* **20**, 034005 (2011).
- [16] W. Tian, K. Tachibana and M.J. Kushner, *J. Phys. D: Appl. Phys.* **47**, 055202 (2014).
- [17] C.E. Brennen, *Cavitation and Bubble Dynamics* (Oxford University Press, New York, 1995).
- [18] D.J. Flannigan and K.S. Suslick, *Nature* **434**, 52 (2005).
- [19] S.I. Nikitenko, *Advances Phys. Chem.* **2014**, 173878 (2014).
- [20] P.-K. Choi, S. Abe and Y. Hayashi, *J. Phys. Chem. B* **112**, 918 (2008).
- [21] Y. Hayashi and P.-K. Choi, *Ultrason. Sonochem.* **23**, 333 (2015).
- [22] M. Virost, R. Pflieger, J. Ravoux and S.I. Nikitenko, *J. Phys. Chem. C* **115**, 10752 (2011).
- [23] Y. Iwata, N. Takada and K. Sasaki, *Appl. Phys. Express* **6**, 127301 (2013).
- [24] K. Yasui, *Ultrason.* **36**, 575 (1998).
- [25] J.-S. Chang, P.A. Lawless and T. Yamamoto, *IEEE Trans. Plasma Sci.* **19**, 1152 (1991).